Magnetic properties of $RbVF_4$

1991 J. Phys.: Condens. Matter 3 2953

(http://iopscience.iop.org/0953-8984/3/17/012)

J. Phys.: Condens. Matter 3 (1991) 2953–2961. Printed in the UK

Magnetic properties of $RbVF_4$

R A Cowley†‡, N Cope†, B Wanklyn†, T E Mason§ and W J L Buyers‡

†Department of Physics, Clarendon Laboratory, Oxford University, Parks Road, Oxford OX1 3PU, UK

‡AECL Research, Chalk River, Ontario, Canada K0J 1J0

§Department of Physics, McMaster University, Hamilton, Ontario, Canada

Received 28 December 1990, in final form 21 February 1991

Abstract. The magnetic and electronic properties of $RbVF_4$ have been studied using infrared absorption spectroscopy and neutron scattering techniques. The V^{+++} ion has in its ground state both orbital and spin angular momentum and so is strongly influenced by the tetragonal and orthorhombic crystal fields. The absorption bands in the infrared have been assigned to transitions between the states of the V^{+++} ion. The neutron scattering measurements determined the nature of the antiferromagnetic order and the low-temperature excitations. The ground state of the V^{+++} ions is a doublet which is split by the magnetic ordering at 44 K. The temperature dependence of the order parameter and the behaviour of the excitations suggest that the magnetic interactions are largely confined to the antiferromagnetic sheets. The excitations observed are not associated with the ground doublet but with transitions from the ground state to the next excited state. Values for the crystal field, spin–orbit and exchange parameters are deduced.

1. Introduction

The magnetic properties of the 3d transition metal ions are very dependent upon the valency of the ion and its local environment. Most of the studies of the spin waves in concentrated materials have been on materials with ions in the second half of the 3d shell such as Mn^{++}, Fe^{++}, Co^{++}, Ni^{++} and most recently Cu^{++}. Relatively little work has been performed on the ions in the first half of the shell, and so in this paper we report on measurements of the excitations in $RbVF_4$, where the V^{+++} ion has two 3d electrons. The results show the importance of spin moments, the effect of the local crystal field, and the exchange interaction.

The crystal structure of $RbVF_4$ is a layer structure in which two-dimensional networks of VF_6 octahedra are separated by Rb ions. The ideal structure is the $TlAlF_4$ tetragonal structure with one formula unit in each unit cell. The V ions are at the origin of the unit cell, the Rb ions at $(\frac{1}{2}, \frac{1}{2}, \frac{1}{2})$ and the F ions at $(\frac{1}{2}, 0, 0)$, $(0, \frac{1}{2}, 0)$ and $(0, 0, \pm u)$ with $u \simeq 0.28$ (Hidaka *et al* 1986). The lattice parameters are approximately $a = b = 0.385$ nm and $c = 0.632$ nm, so the V–F bonds are 0.192 nm long in the ab plane and 0.178 nm along c. Each V ion is then surrounded by a tetragonal environment of F ions. In practice $RbVF_4$ does not have this ideal structure (Hidaka *et al* 1984), but the structure is distorted by rotations of the F octahedra about the a, b and c axes together with a displacement of the Rb ions along the c axis. Below 184K superlattice reflections are observed

0953-8984/91/172953 + 09 $03.50

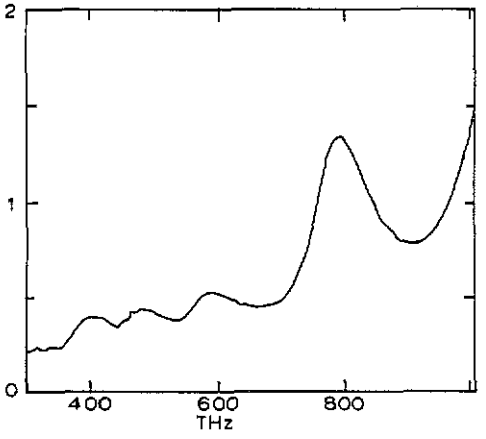

Figure 1. The absorption spectrum of $RbVF_4$ in the near infrared at 9K. The vertical scale is arbitary and the horizontal scale is frequency.

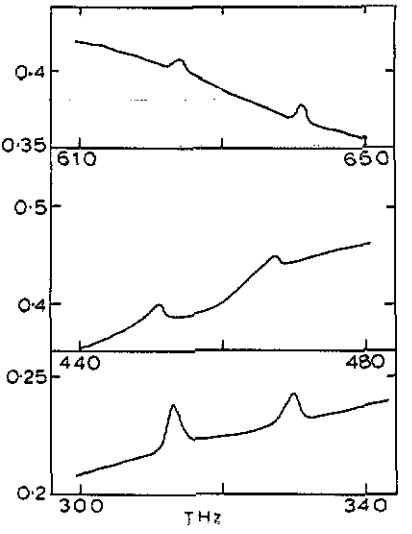

Figure 2. Details of the absorption spectrum of $RbVF_4$ at 9K to show the sharp peaks. Some of these measurments were performed with samples of different thicknesses from those used for the results in figure 1.

corresponding to wavevectors, $(\frac{1}{2}, \frac{1}{2}, 0)2\pi/a$, $(\frac{1}{2}, 0, 0)2\pi/a$ and $(0, \frac{1}{2}, 0)2\pi/a$ where as throughout this paper, we shall refer all wavevectors to the reciprocal lattice of the ideal unit cell. The unit cell has small distortions, of order 0.36%, to give an orthorhombic structure. As far as we are aware the detailed low-temperature crystal structure of $RbVF_4$ has not been determined; it is, however, likely to be similar to that of $CsVF_4$ for which Hidaka *et al* (1986) determined rotations of about 7° about the *c* axis and 5° about the *a* and *b* axes. The local environment of each V ion is then based on an octahedral arrangement of six F ions with a large tetragonal distortion and a smaller orthorhombic distortion due to the F rotations. We discuss the effect of this structure on the energy levels of the V ions in the next section, and also describe infrared measurements of the absorption spectra.

Neutron scattering measurements of the magnetic structure and low-energy excitations were performed at Chalk River Laboratories. There is an antiferromagnetic transition at 44K with a wavevector described by $(\frac{1}{2}, \frac{1}{2}, 0)2\pi/a$, showing that the moments align parallel to one another in successive V–F planes. This is the same structure as found in $CsVF_4$ (Hidaka *et al* 1990) when a magnetic field of 2T is applied along the *c* axis. The results and those for the excitations are described and discussed in section 3.

2. Single-ion properties

2.1. Infrared measurements

The infrared absorption spectrum of $RbVF_4$ was measured using a Perkin–Elmer Lambda 9 spectrophotometer. The results for incident photon frequencies between 300 and 1000 THz with the sample cooled to 9K are shown in figure 1. They show four broad peaks at the frequencies listed in table 1. On raising the temperature the frequencies of these peaks were essentially independent of temperature. A more careful study of the

Table 1. Frequencies of the transitions observed in the infrared spectrum at 9K. (*a*) Broad features. (*b*) Sharp weak features.

	Observed frequencies			
	(cm^{-1})	(THz)	Assignment	Calculated (THz)
(*a*)	26 400 ± 300	792 ± 10	$^3A_2$ — $^3T_1$	792
	19 600 ± 300	588 ± 10	^3E	513
	16 000 ± 400	480 ± 12	^3E — $^3T_2$	555
	13 200 ± 400	396 ± 12	$^3B_2$	396
(*b*)	21 420 ± 30	642 ± 1		
			$^1A_1$	620
	20 820 ± 30	625 ± 1	^1E	
	15 580 ± 30	467 ± 1		
			$^1B_2$	269
	15 000 ± 30	450 ± 1		
	11 080 ± 30	322 ± 1		
			$^1A_2$ or ^1E—$^1T_1$	262
	10 470 ± 30	314 ± 1		

spectra also shows three sharp doublets, as shown in figure 2, with frequencies as indicated in table 1. All of the doublets have the same splitting, namely 17.5 ± 1 THz. On warming this structure became less distinct, and could not be observed with the sample above 80K.

2.2. *Theory of the V^{+++} ion*

There are two 3d electrons in the V^{+++} ion, and its properties in a cubic crystal field were calculated by Tanabe and Sugano (1954), by Liehr and Ballhausen (1959) and have been reviewed by McClure (1959) and by Abragam and Bleaney (1970). Analogous calculations in a tetragonal crystal field were performed by Maki (1958). We shall make use of their results without giving a detailed derivation. The ground state of the free V^{+++} ion is a ^3F state ($L = 3$, $S = 1$), and in a weak cubic crystal field this sevenfold orbitally degenerate state is split into a $^3T_1$ ground state and $^3T_2$ and $^3A_2$ excited states. In $RbVF_4$, however, the crystal field splittings are not small, but are comparable with the energy differences between the ^3F state and the excited free-ion states, ^1D, ^3P, ^1G and ^1S. Consequently the optical spectrum, figure 1, can only be obtained if both these higher states and the crystal field effects are included. Figure 2 shows a schematic diagram of the splittings of the different states in a weak crystalline field but in practice there is considerable mixing between the states of the same symmetry.

The optical spectra of V^{+++} ions in solution show three absorption bands at 522 THz, 762 THz and 1035 THz which are assigned to transitions from the $^3T_1$ ground state to the $^3T_2$, $^3T_1$ and $^3A_2$ excited states. By analogy with these results we can assign the results

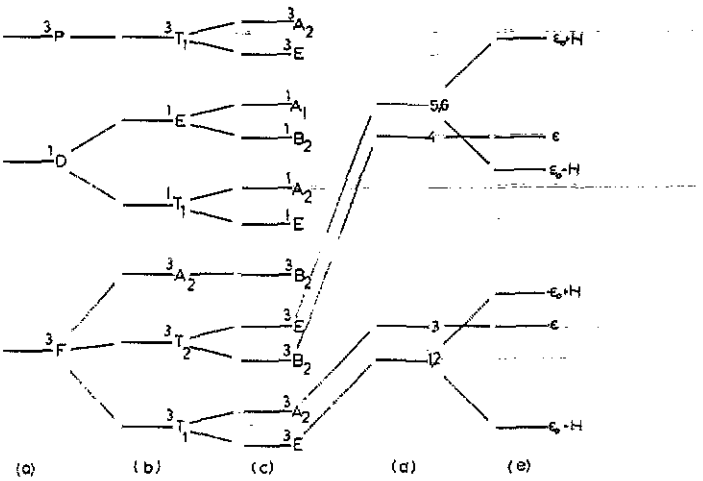

Figure 3. Schematic energy level diagram for V^{+++} ion, (a) free (b) in a weak octahedral field, (c) in a tetragonal field, (d) in the orthohombic and spin–orbit fields and (e) in a molecular magnetic field. The labels in (a)–(c) are symmetry labels while those for (d) and (e) are energies.

shown in figure 1 and table 1. The rise at the high-frequency end is associated with a transition to the $^3A_2$ state, while the four peaks in figure 1 are associated with transitions to the $^3T_2$ and $^3T_1$ excited states which are both split by the large tetragonal distortion of the crystal field as shown in figure 3.. The cubic crystal field parameter can then be estimated by treating the Coulomb interactions as given by McClure (1959), and assuming that there is a simple splitting of the cubic crystal field by the tetragonal distortion. The levels so deduced are given in table 1 for a cubic crystal field parameter $10Dq = 490$ THz. These results are then reasonably consistent with the experimental results if we assume there is a simple level repulsion between the two E levels, raising one in frequency by 75 THz and reducing the other by the same amount.

The weak sharp features in the spectrum arise from transitions in which the spin quantum number changes. For all three of the features there is a doublet with a splitting of 17.5 THz, and so it is reasonable to suppose that this splitting arises in the $^3T_1$ ground state. The transitions then arise from the ground state to a $^1A_1$ state with a frequency in good agreement with the model, and to the $^1T_1$ and ^1E states both of which are split by the tetragonal field, and within the energy interval available in the experiment only one of each of the tetragonal-split states is observable. These considerations then provide a consistent explanation of the infrared spectra in figures 1 and 2, with a reasonable value of the cubic crystal field parameter, but with large splittings, 280, 160 and 279 THz, of the excited states by the tetragonal crystal field.

2.3. The ground state

The results of the previous section are consistent with the theoretical calculations which suggest that the ground state of the V^{+++} ion in an octahedral crystal field is a $^3T_1$ state. These states can be described by an effective orbital angular momentum, $l = 1$, and have spin, $S = 1$. The matrix element of the orbital angular moment, L, are then given by the matrix elements of l multiplied by a constant, $-\alpha$, where in the weak-crystal-field case $\alpha = 1.5$ and in a stronger crystal field α is probably smaller.

Table 2. The wavefunctions $|l_z S_z\rangle$ and energies of the ground state manifold of the V^{+++} ion in $RbVF_4$. Here $\varepsilon_0 = (\varepsilon^2 + \lambda^2)^{1/2}$, $F = \varepsilon_0 + \alpha\lambda$, $G = \varepsilon_0 - \alpha\lambda$, $N_1 = (\varepsilon^2 + F^2)^{1/2}$, $N_2 = (\varepsilon^2 + G^2)^{1/2}$.

Label	Energy	Wavefunction
1	$-\varepsilon_0$	$N_1(\varepsilon\|1\bar{1}\rangle - F\|\bar{1}1\rangle)$
2	$-\varepsilon_0$	$N_1(\varepsilon\|\bar{1}1\rangle - F\|1\bar{1}\rangle)$
3	$-\varepsilon$	$(1/\sqrt{2})(\|\bar{1}0\rangle - \|10\rangle)$
4	ε	$(1/\sqrt{2})(\|\bar{1}0\rangle + \|10\rangle)$
5	ε_0	$N_2(\varepsilon\|1\bar{1}\rangle + G\|\bar{1}1\rangle)$
6	ε_0	$N_2(\varepsilon\|\bar{1}1\rangle + G\|1\bar{1}\rangle)$

The effective Hamiltonian within the ground state manifold can then be written as

$$\mathcal{H}_{\text{eff}} = -C(l_z^2 - 1) + (\varepsilon/2)\left[(l^+)^2 + (l^-)^2\right] - \alpha\lambda \boldsymbol{l}\cdot\boldsymbol{S} \tag{2.1}$$

where the first term is the tetragonal distortion of the crystal field, the second is the smaller orthorhombic distortion and λ is the spin–orbit interaction and its free-ion value is about 3 THz (McClure 1959, Abragam and Bleaney 1970).

The tetragonal distortion leads to a splitting of the orbital triplet, T_1, state to give the state with $l_z = 0$ a higher energy than those with $l_z = \pm 1$ by an energy of C. The doubly degenerate orbital ground state and the three spin states are then a manifold of six states within which the effective Hamiltonian can be diagonalized to give the eigenvalues and eigenvectors shown in table 2.

The infrared experiments suggest that there is an energy separation within the ground manifold of 17.5 THz. This is substantially larger than the spin–orbit splitting or the frequency associated with the Néel temperature, 0.92 THz. Consequently the splitting must arise from the crystal fields. There are two possible causes. Firstly, it could arise from the tetragonal splitting, C, of (2.1), but its magnitude is much less, $\simeq \frac{1}{10}$, than the tetragonal splittings of the excited states and it is difficult to understand the reason for this. Secondly, if C is ~100 THz, the splitting could arise from the orthorhombic distortion ε, of (2.1). In the case $\varepsilon \simeq 8$ THz, and is larger than $\alpha\lambda$, so the energy levels in table 2 are approximately ε and $-\varepsilon$, giving $\varepsilon \simeq 8$ THz. In the next section we shall explain that this alternative is the more likely.

3. Magnetic cooperative phenomena

3.1. Neutron scattering measurements

The neutron scattering measurements were performed on the L3 triple-axis crystal spectrometer at the NRU reactor of Chalk River Laboratories. Squeezed Si monochromators were used to provide the incident monochromatic beam and to analyse the scattered beam, whose frequency was kept fixed at 3, 3.5, 4.5, 6 or 7 THz. The single crystal of $RbVF_4$ was mounted in a variable-temperature cryostat so that the (110) crystallographic axis was vertical. The temperature could be controlled with an accuracy of ±0.1 K.

Initially measurements were made by using the spectrometer to study the elastically scattered neutrons along the line $(\frac{1}{2}, \frac{1}{2}, \eta)$ in reciprocal space, while the crystal was cooled. The results showed a rapidly increasing intensity at $(\frac{1}{2}, \frac{1}{2}, 0)$ below 44K, which we

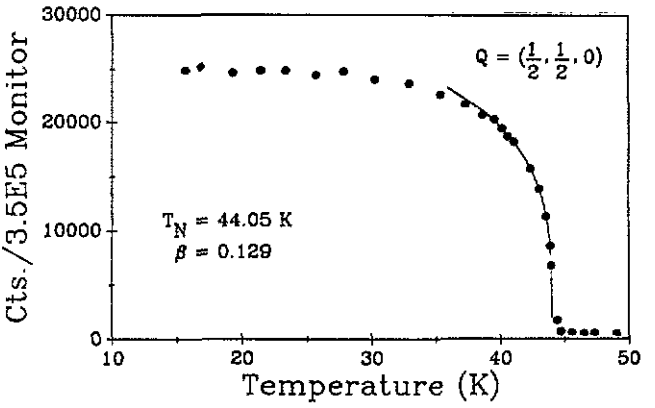

Figure 4. The temperature dependence of the $(\frac{1}{2},\frac{1}{2},0)$ antiferromagnetic Bragg reflection in $RbVF_4$. The line is a least-squares fit to a power law of the form $(T_N - T)^{2\beta}$.

interpret as being due to the onset of long-range antiferromagnetic order. Above 44K there is a weak (twice the background) reflection at $(\frac{1}{2}, \frac{1}{2}, 0)$. This probably arises because of the F rotations about the c axis. In the ideal state these motions have zero structure factor, but the rotations about the *a* and *b* axes give rise to small distortions which account for this weak scattering. The width of the Bragg reflection along the $(\frac{1}{2}, \frac{1}{2}, \eta)$ line is consistent with the development of complete three-dimensional magnetic order.

The results show that the two-dimensional order of the magnetic moments on the V ions is similar to that found in other layer structures, such as K_2NiF_2 and $CsVF_2$ (Hidaka *et al* 1990). The stacking of the antiferromagnetic planes is, however, different from that in $CsVF_4$ in zero applied field although the $RbVF_4$ arrangement is preferred in $CsVF_4$ when a field in excess of 0.4T is applied along the *c* axis.

The temperature dependence of the $(\frac{1}{2}, \frac{1}{2}, 0)$ Bragg reflection is shown in figure 4. This has been fitted to the power law $(T_N - T)^{2\beta}$, with the result that close to T_N, $(T_N - T)/T_N < 0.1$, $\beta = 0.129 \pm 0.01$ and $T_N = 44.05 \pm 0.10$K. The value of β is within error consistent with that expected, 0.125, for a two-dimensional Ising model suggesting that the critical fluctuations have two-dimensional character.

Measurements were made of the critical scattering at $(\frac{1}{2}, \frac{1}{2}, \eta)$ for various η as a function of temperature. Unfortunately the large incoherent elastic scattering from the V ions produced a large temperature-independent background, which effectively prevented a quantitative study of the critical scattering. We were nevertheless able to confirm that the critical scattering showed approximately two-dimensional character.

The magnetic excitations were studied at low energies by means of inelastic scans with the wavevector transfer held constant. A typical result in figure 5, shows a well defined neutron group at 4.2K which is no longer present above the magnetic ordering transition at 46K. This shows that the scattering arises from a magnetic excitation. The dispersion relation for these excitations is shown in figure 6 for excitations propagating along the (00η) and $(\zeta\zeta 0)$ directions. In the former case there is, within error, no dispersion showing that the inter-plane exchange interactions are very small; in the latter case there is significant dispersion corresponding to strong interactions within the planes.

A simple model of the spin-wave dispersion relationship for a two-dimensional antiferromagnet for spin waves propagating along $(\zeta\zeta 0)$ gives

$$\omega(\zeta)^2 = (\Delta + K)^2 - K^2 \cos^2(2\pi\zeta) \tag{3.1}$$

A least-squares fit to the observed dispersion gives the gap term

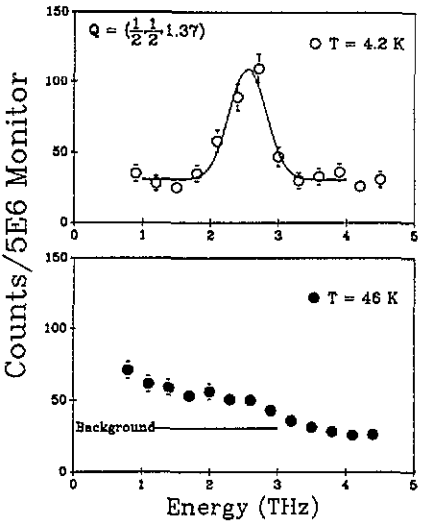

Figure 5. Neutron scattering from $RbVF_4$. The peak at 4.2K arises from a magnetic excitation and disappears on heating above the Néel temperature.

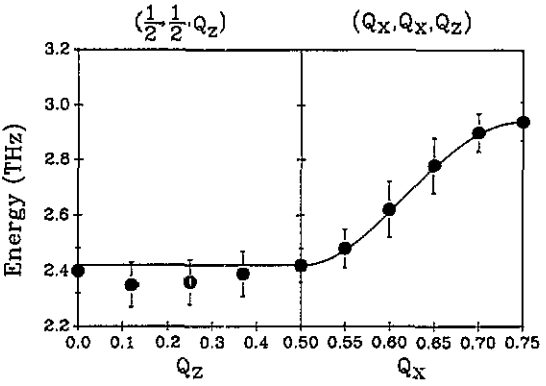

Figure 6. The dispersion relation for the low-energy magnetic excitations in $RbVF_4$.

$$\Delta = 1.27 \pm 0.05 \text{ THz}$$

and the exchange term

$$K = 1.67 \pm 0.05 \text{ THz}$$

Experiments were also performed to investigate if there were excitations of higher frequency. Scans with frequency transfers up to 12.5 THz did not show any appreciable inelastic scattering.

3.2. Analysis of the results

The simplest approximation via which to take account of the interactions between the magnetic moments is the molecular field theory. If the exchange interaction between nearest neighbours is of the form

$$\mathcal{H}_{ex} = \tfrac{1}{2} J \sum_{ij} \boldsymbol{S}_i \cdot \boldsymbol{S}_j \tag{3.2}$$

then the molecular field on site i is

$$H_M = zJ\langle S^z \rangle.$$

The ground state of the system is therefore state 1, and at low temperatures $\langle S^z \rangle = \pm 1$, so $H_M = 4J$.

The transverse terms in the Hamiltonian depend on S^+ and S^- which have no matrix elements between the two states 1 and 2 on which the ordering depends. If the splitting between these states and the states 3–6 is sufficiently large that the latter can be neglected, the system is then identical to that of a two-dimensional Ising model with nearest-neighbour interactions for which the exchange constant and transition temperature are related by $kT_N = 2.261J$. Using the measured value of T_N this leads to a value of $J =$

0.4 THz. The higher-energy states, 3–6, are likely to reduce the tendency towards magnetic order and so this estimate of J may be somewhat small.

Because the neutron scattering amplitude is proportional to the operator $\boldsymbol{L} + \boldsymbol{S}$, it is unable to probe transitions between the states 1 and 2. The excitations observed in figures 5 and 6 cannot therefore arise from normal spin waves between members of the ordering states. Neutron scattering can, however, study transitions between the states 1 and 3, 1 and 4, and 1 and 5.

Suppose, for the present, we consider transitions between states 1 and 3. Pseudo-boson theory can be used to evaluate the dispersion relation for the excitations with the result that they are given by (3.1) with

$$K = [2(\varepsilon + F)^2/(\varepsilon^2 + F^2)]J \tag{3.3}$$

and

$$\Delta = \varepsilon_0 - \varepsilon. \tag{3.4}$$

Using the value of K deduced from figure 6, and J from T_N we obtain from (3.3) that

$$\varepsilon^2 + F^2 = 0.48\,(\varepsilon + F)^2.$$

This is most closely satisfied if $F \simeq \varepsilon$ which implies that $\alpha\lambda \ll \varepsilon$, and hence the 17.5 THz splittings observed in the infrared spectrum arise from the orthorhombic crystal field parameter, ε. The transitions between states 1 and 4 and 1 and 5 were not then observed in the neutron scattering experiments because they have larger frequencies than were available experimentally.

The alternative scenario is to assume that ε is small, when (3.3) predicts that $K \simeq 2J$, which is inconsistent with the experimental results.

The strength of the crystal field and spin–orbit parameters can now be estimated if we assume that the sharp features in the infrared spectrum arise from spin-conserving transitions when $2\varepsilon_0 = 17.5$ THz and that $\varepsilon_0 - \varepsilon = 1.27$ THz. The orthorhombic crystal field parameter ε is then given by 7.5 ± 0.5 THz and the spin–orbit parameter $\alpha\lambda = 4.5 \pm 0.5$ THz, while the nearest-neighbour exchange interaction $J = 0.40 \pm 0.04$ THz. These values then give the ratio of $(\varepsilon^2 + F^2)/(\varepsilon + F)^2$ as 0.54 which is within the uncertainties consistent with the experimental results.

4. Conclusions

In the previous sections we have presented a detailed study of the magnetic properties of $RbVF_4$, which is of interest because it is necessary to take account of the crystal field levels of the V^{+++} ion in detail. Measurements were made of the absorption bands in the infrared spectrum and these enabled the cubic crystal field term $10Dq$ to be determined as 480 THz which can be compared with the value of 560 THz deduced for V^{+++} ions in corundum (McClure 1959). The levels produced by the cubic field are then split by a large tetragonal distortion which produces splittings of these levels ~100 THz depending on the particular states involved.

The magnetic ordering and low-energy excitations were studied by neutron scattering techniques. The antiferromagnetic ordering was similar to that of other layered materials of the same structure in that the in-plane exchange constant are much larger than the inter-plane interactions. The system is, however, different from $S = \frac{1}{2}$ Ising system such as Rb_2CoF_4 (Ikeda and Hutchings 1978) because the magnetic excitations observed do

not arise from transitions within the ground state doublet but from transitions between the ground state and the first excited state. A careful analysis of the results enabled us to deduce the orthorhombic crystal field parameter as 7.5 ± 0.5 THz, and the spin–orbit parameter $\alpha\lambda = 4.5 \pm 0.5$ THz. This is in surprisingly good agreement with the free-ion spin–orbit interaction of 3.13 THz when multiplied by the small-crystal-field effective orbital factor $\alpha = 1.5$.

Further work is needed to calculate the crystal field parametes from first principles and also to measure the excitations to the higher crystal field levels.

Acknowledgments

We are grateful to Dr F L Pratt for help with the infrared measurements. RAC is pleased to acknowledge the hospitality of AEC Research, Chalk River. Financial support was provided by the UK Science and Engineering Research Council, by the Natural Sciences and Engineering Research Council of Canada, and Atomic Energy of Canada Ltd.

References

Abragam A and Bleaney B 1970 *Electron Paramagnetic Resonance of Transition Ions* (Oxford: Oxford University Press)
Hidaka M, Fujii H, Garrard B J and Wanklyn B M 1984 *Phys. Status Solidi* a **86** 75
—— 1986 *Phys. Status Solidi* a **96** 413, 415
Hidaka M, Fujii H, Nishi M and Wanklyn B M 1990 *Physica* B **160** 281
Ikeda H and Hutchings M T 1978 *J. Phys. C: Solid State Phys.* **11** L529
Liehr A D and Ballhausen C J 1959 *Ann. Phys., NY* **6** 134
Maki G 1958 *J. Chem. Phys.* **28** 651
McClure D S 1959 *Solid State Physics* vol 9, ed F Seitz and D Turnbull (New York: Academic)
Tanabe Y and Sugano S 1954 *J. Phys. Soc. Japan* **9** 753, 766